ADVANCES IN ATMOSPHERIC SCIENCES, VOL. 27, NO. 5, 2010, 1051–1063

The Vertical Structures of Atmospheric Temperature Anomalies Associated with El Niño Simulated by the LASG/IAP AGCM: Sensitivity to Convection Schemes

ZHANG Jie[1,2,3] (张 洁), ZHOU Tianjun*[1] (周天军), BAO Qing[1] (包 庆), and WU Bo[1] (吴 波)

[1] *State Key Laboratory of Numerical Modeling for Atmospheric Sciences and Geophysical Fluid Dynamics, Institute of Atmospheric Physics, Chinese Academy of Sciences, Beijing* 100029

[2] *Graduate University of Chinese Academy of Sciences, Beijing* 100049

[3] *Laboratoire de Météorologie Dynamique/CNRS, Université Paris* 6*, France*

(Received 27 September 2009; revised 12 January 2010)

ABSTRACT

The vertical structures of atmospheric temperature anomalies associated with El Niño are simulated with a spectrum atmospheric general circulation model developed by LASG/IAP (SAMIL). Sensitivity of the model's response to convection scheme is discussed. Two convection schemes, i.e., the revised Zhang and Macfarlane (RZM) and Tiedtke (TDK) convection schemes, are employed in two sets of AMIP-type (Atmospheric Model Intercomparison Project) SAMIL simulations, respectively. Despite some deficiencies in the upper troposphere, the canonical El Niño-related temperature anomalies characterized by a prevailing warming throughout the tropical troposphere are well reproduced in both simulations. The performance of the model in reproducing temperature anomalies in "atypical" El Niño events is sensitive to the convection scheme. When employing the RZM scheme, the warming center over the central-eastern tropical Pacific and the strong cooling in the western tropical Pacific at sea surface level are underestimated. The quadru-pole temperature anomalies in the middle and upper troposphere are also obscured. The result of employing the TDK scheme resembles the reanalysis and hence shows a better performance. The simulated large-scale circulations associated with atypical El Niño events are also sensitive to the convection schemes. When employing the RZM scheme, SAMIL failed in capturing the classical Southern Oscillation pattern. In accordance with the unrealistic anomalous Walker circulation and the upper tropospheric zonal wind changes, the deficiencies of the precipitation simulation are also evident. These results demonstrate the importance of convection schemes in simulating the vertical structure of atmospheric temperature anomalies associated with El Niño and should serve as a useful reference for future improvement of SAMIL.

Key words: temperature anomalies, El Niño, simulation, convection schemes

Citation: Zhang, J., T. J. Zhou, Q. Bao, and B. Wu, 2010: The vertical structures of atmospheric temperature anomalies associated with El Niño simulated by the LASG/IAP AGCM: Sensitivity to convection schemes. *Adv. Atmos. Sci.*, **27**(5), 1051–1063, doi: 10.1007/s00376-010-9167-3.

1. Introduction

The convection scheme has been one of the critical issues for the simulation of the current climate. Although simulations by atmospheric general circulation models (AGCMs) with different convection schemes are comparable, the concepts and tunable parameters behind the schemes are quite different from one to another (Arakawa, 2004). Zhang (1994) investigated the effects of cumulus convection and found significant effects on the monsoon circulation and the associated precipitation. Yhang and Hong (2008) indicate that modifications of the convection scheme dominate the improvements in simulating summer monsoon circulations over East Asia. The skills of the simulations with different schemes are also highly temporal and

*Corresponding author: ZHOU Tianjun, zhoutj@lasg.iap.ac.cn

regional dependent (Liang et al., 2004a; Fernández et al., 2007; Zhu and Liang, 2007).

Convection has a great impact on the heating profile through the release of latent heat by condensation in the tropics, and has a profound impact on vertical stability as well as the large-scale circulation. Previous studies on the model sensitivity to the choice of convection schemes mainly highlight the differences in climatologies of physical variables, especially for precipitation and the large-scale circulation (Giorgi and Shields, 1999; Wang et al. 2009; Xu et al. 2009; Li et al. 2010; Chen et al., 2010). Less attention has been paid to the temperature in previous model evaluations. By examining the tropical vertical temperature structure in the 40-yr ECMWF Re-Analysis data (ERA-40, Uppala et al., 2005), Trenberth and Smith (2006) find two rather different vertical structures of temperature anomalies associated with different flavors of El Niño. The first is the canonical El Niño mode that captures the 1982/83, 1986/87, and 1997/98 El Niño events in contrast to the 1988/89 La Niña event, and the second is the atypical El Niño mode featuring the prolonged warm ENSO phase during the early 1990s. These two modes can generally be replicated by the Japanese Reanalysis (JRA-25, Onogi et al., 2007) with somewhat modified form for the atypical El Niño mode (Trenberth and Smith, 2009).

Great efforts have been devoted to the development of AGCMs in the State Key Laboratory of Numerical Modeling for Atmospheric Sciences and Geophysical Fluid Dynamics at the Institute of Atmospheric Physics (LASG/IAP) in the past decades (see Zhou et al., 2007 for a review). The spectral model of LASG/IAP named SAMIL has been widely used in East Asian monsoon (Chen et al., 2009), global monsoon (Zhang et al., 2008), and air-sea interaction studies (Li et al., 2009; Wu et al., 2009). However, the performance of the model in simulating the vertical structure of temperature anomalies associated with El Niño is still unknown. The present study aims to answer the following questions: How is the performance of the LASG/IAP AGCM in simulating the vertical temperature anomalies associated with El Niño? Are the two anomalous temperature structures reproducible with the LASG/IAP AGCM forced by historical sea surface temperature (SST)? What is the sensitivity of LASG/IAP AGCM to convection schemes?

The rest of the paper is organized as follows. Section 2 describes the model, convection schemes, experimental design, and analysis method. Impacts of different convection schemes on the reproduction of the temperature anomalies associated with two types of El Niño are investigated in section 3. The associated circulations and precipitation changes are discussed in section 4. Conclusions are presented in section 5.

2. Model, convection schemes, experimental design, and analysis method

2.1 *Model description*

The LASG/IAP AGCM SAMIL is rhomboidally truncated at zonal wave number 42 (R42 horizontal resolution). This truncation is equivalent to a horizontal grid size of 2.8125° in longitude and 1.66° in latitude. The vertical axis is a classical hybrid σ-p vertical coordinate and has 26 levels, up to about 2.1941 hPa. Both the updated Slingo Diagnosed Cloud Scheme (Edwards and Slingo, 1996) and Dai's Low-level Cloud Parameterization Scheme are used (Dai et al., 2005). The Revised UKMO radiation parameterization that takes account of the effects of many kinds of greenhouse gases and aerosols is also adopted (Johns et al., 2004). The land surface model NCAR_CLM (Bonan, 1998) is coupled with SAMIL (Bao et al., 2006). Further information regarding the model can be found in Zhou et al. (2005a, b).

2.2 *Convection schemes*

Two different convection schemes are employed in SAMIL: the revised Zhang-McFarlane convection scheme (Zhang, 2002) and the Tiedtke convection scheme (Tiedtke, 1989) modified by Song (2005). The Zhang and McFarlane (1995) convection scheme is a mass flux convection scheme, based on a plume ensemble concept. It assumes that an ensemble of convective-scale updrafts with associated saturated downdrafts may exist when the atmosphere is conditionally unstable in the lower troposphere, and that all plumes have the same upward mass flux at the base of the convective layer. The closure is based on the Arakawa-Schubert quasi-equilibrium (Arakawa and Schubert, 1974). Convection occurs when there is positive convective available potential energy (CAPE) and the CAPE will be removed at an exponential rate with a specified adjustment time scale. In the updated version, the closure assumption is revised (Zhang, 2002), which proposes a quasi-equilibrium between the convective and the large-scale processes in the free troposphere above the boundary layer.

The Tiedtke scheme is also a mass flux convection scheme (Tiedtke, 1989) considering a population of clouds and the cumulus downdrafts. It is a comprehensive scheme that can represent deep, midlevel, and shallow convection. The closure assumptions for the deep and midlevel convection are maintained by large-scale moisture convergence while the shallow convection is sustained by the supply of moisture derived from surface evaporation. The Tiedtke scheme in

SAMIL identifies the cloud top height and improves the organized outflow (Song, 2005).

Although both the Zhang-McFarlane and Tiedtke convective schemes are based on the mass flux concept, they have evident differences in the closure assumption, the identification of the cloud top height, and the threshold for triggering convection. The major difference between these two schemes is that the Zhang and McFarlane convection scheme only parameterizes deep convection and the Tiedtke scheme considers various types of convection. That is, when the Zhang and McFarlane convection scheme is employed, it should be applied in conjunction with a shallow convection scheme. In SAMIL, the Hack (1994) scheme is employed together with the revised Zhang and McFarlane convection scheme to describe the physical processes of convection.

2.3 *Experimental design*

Two AMIP-type (Atmospheric Model Intercomparison Project) simulations are carried out with two different mass-flux convection schemes now available in SAMIL: the first is the revised Zhang and McFarlane convection scheme (Zhang and McFarlane, 1995; Zhang, 2002; Liu, 2008; hereafter RZM scheme); the second is revised Tiedtke scheme (Tiedtke, 1989; Song, 2005; hereafter TDK scheme). As in standard AMIP runs, identical SST and sea ice concentration (SIC) during the AMIP II period (from 1976 to 1999) are employed in both simulations.

The model simulation covers the period from January 1976 to December 1999. The SST and SIC are adopted from PCMDI (Program for Climate Model Diagnosis and Inter-comparison, http://www-pcmdi.llnl.gov/). The three-dimensional aerosol distributions are derived from a global aerosol climate model SPRINTARS (Spectral Radiation-Transport Model for Aerosol Species, Takemura et al., 2000). Only the direct effects of aerosols are considered. The first five years were discarded as the spin-up stage, so that the period 1981–1999 is used in this study.

The following datasets are used for the validation of model results: (1) the ERA-40 reanalysis dataset (Uppala et al., 2005); (2) the precipitation data sets from the Global Precipitation Climatology Project (GPCP, Adler et al., 2003); (3) the monthly datasets of SST from the Hadley Centre Global Sea Ice and Sea Surface Temperature (HadISST) (Rayner et al., 2003).

2.4 *Analysis method*

An empirical orthogonal function (EOF) analysis is performed in the manner used in Trenberth and Smith (2006) to get the signals of different flavors of El Niño. Nine levels (1000, 850, 700, 600, 500, 400, 300, 200, and 100 hPa) of monthly temperature from January 1981 to December 1999 were chosen as primary levels. In order to avoid possible contamination by the primarily extratropical sources of variability, the region of the tropics from 30°N to 30°S is defined as the core region in which to perform the EOF analysis. All months are selected and the annual cycle is removed before performing EOF analysis. Although the selected time span is not exactly the same as that used in Trenberth and Smith (2006), the results are not changed much, indicating insensitivity to the dates selected. The results can also be derived from the independent reanalysis dataset JRA-25 (Trenberth and Smith, 2009).

The ENSO-related EOF modes derived from ERA-40 reanalysis are used as benchmarks. The covariant anomaly fields associated with the typical modes of EOF are obtained from linear regression with the mode's principal components. For a quantitative comparison, the model outputs were mapped onto the ERA-40 grids using inverse distance weighted interpolation.

3. Results

To generally assess the model's performance in reproducing the observed temperature variability, we first compare standard deviations of monthly temperature from the ERA-40 reanalysis with the same quantities from the simulations. In the reanalysis, the standard deviation (STD) of monthly temperature variability is zonally symmetric, showing a minimum in the tropical troposphere and a maximum in the extratropical stratosphere (Fig. 1a). The STD is reasonably reproduced in the lower and middle troposphere but is overdeveloped above 100 hPa. Since the overestimations are evident in both simulations, we only focus on the temperature variability below 100 hPa.

3.1 *The leading EOF modes in SAMIL simulations*

We use the EOF results derived from ERA-40 as observational evidence to evaluate the model performance. Before the evaluation, the second EOF mode in ERA-40 is eliminated, as this is considered to be a spurious mode and apparently arises from problems with bias adjustment in assimilating data (Trenberth and Smith, 2006, 2009). The third EOF mode in ERA-40 is related to the atypical El Niño events and is considered as the second nontrivial leading mode hereafter.

The percentages of overall variance accounted for by the first six eigenvalues of the EOF analysis in the simulations are shown in Fig. 2. The first (second)

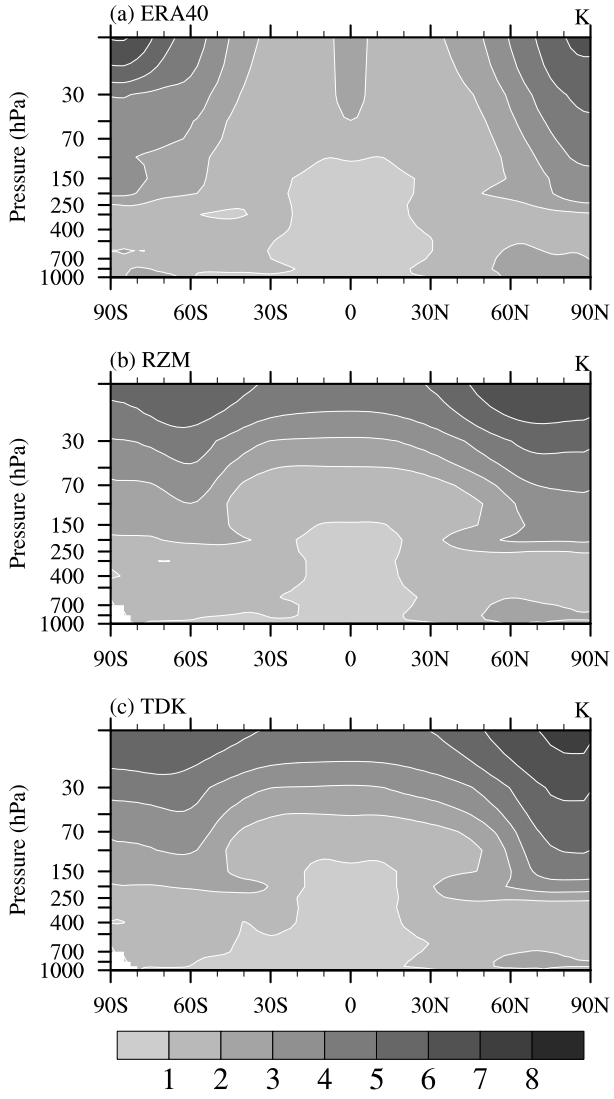

Fig. 1. Zonal mean of the monthly anomaly temperature standard deviation as a latitude–height cross section derived from (a) ERA40, (b) experiment using the revised Zhang and Macfarlane convective scheme (RZM), and (c) experiment using the revised Tiedtke convective scheme (TDK). Units: K.

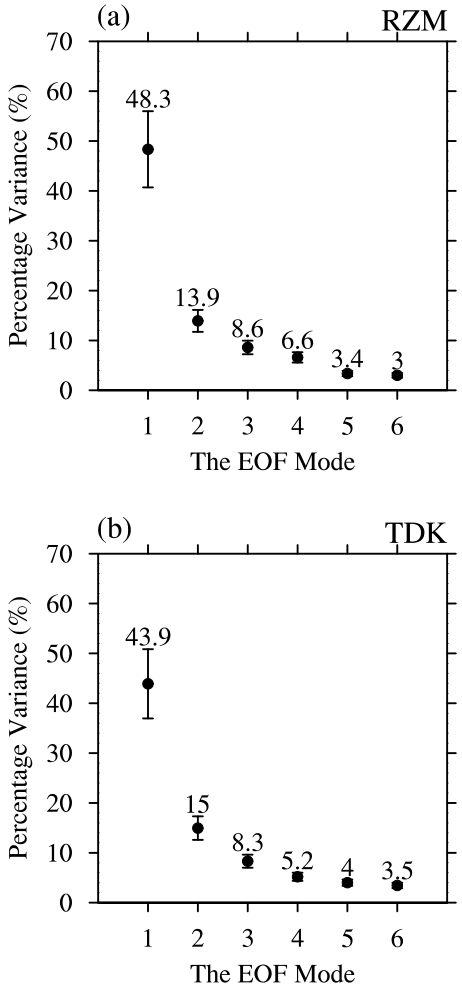

Fig. 2. Percentage variance (%) explained by the first six EOF modes of temperature anomalies obtained from (a) RZM and (b) TDK. The bars represent one standard deviation of the sampling errors.

mode accounts for 48.3% (13.9%) of the variance in RZM and 43.9% (15%) in TDK. According to the rule of North et al. (1982), these first two leading modes are distinguishable from each other as represented by the sampling error bars in Fig. 2. The percentages of the explained deviation start to level off starting with EOF-3. The first two modes dominate the interannual variations and explain about 60% of the total variation in both RZM and TDK. We therefore focus on the first two EOF modes in the following sections.

The spatial patterns of the corresponding zonal mean vertical temperature anomalies are shown in Fig. 3. In the reanalysis (Fig. 3a and Fig. 3b), the dominant features of EOF-1 are the strong warming throughout the tropical troposphere, showing a peak positive value in the middle and upper troposphere. For EOF-2, slight tropical warming and a subtropical cooling dipole straddling the equator are evident in the middle and lower troposphere.

The dominant spatial patterns (EOF-1) are well simulated by the RZM and TDK runs (Fig. 3c and Fig. 3e). Although the mid-latitude cooling in the upper troposphere in the northern and southern hemispheres is insignificant in both simulations, the strong warming in the core region of the tropics from 30°N to 30°S is well captured. For EOF-2 (Fig. 3d and Fig. 3f), the slight warming in the tropical troposphere is reasonably reproduced in both simulations. However, the subtropical cooling in the middle troposphere is too strong, and the subtropical warming in the lower stratosphere extends too far poleward in both hemi-

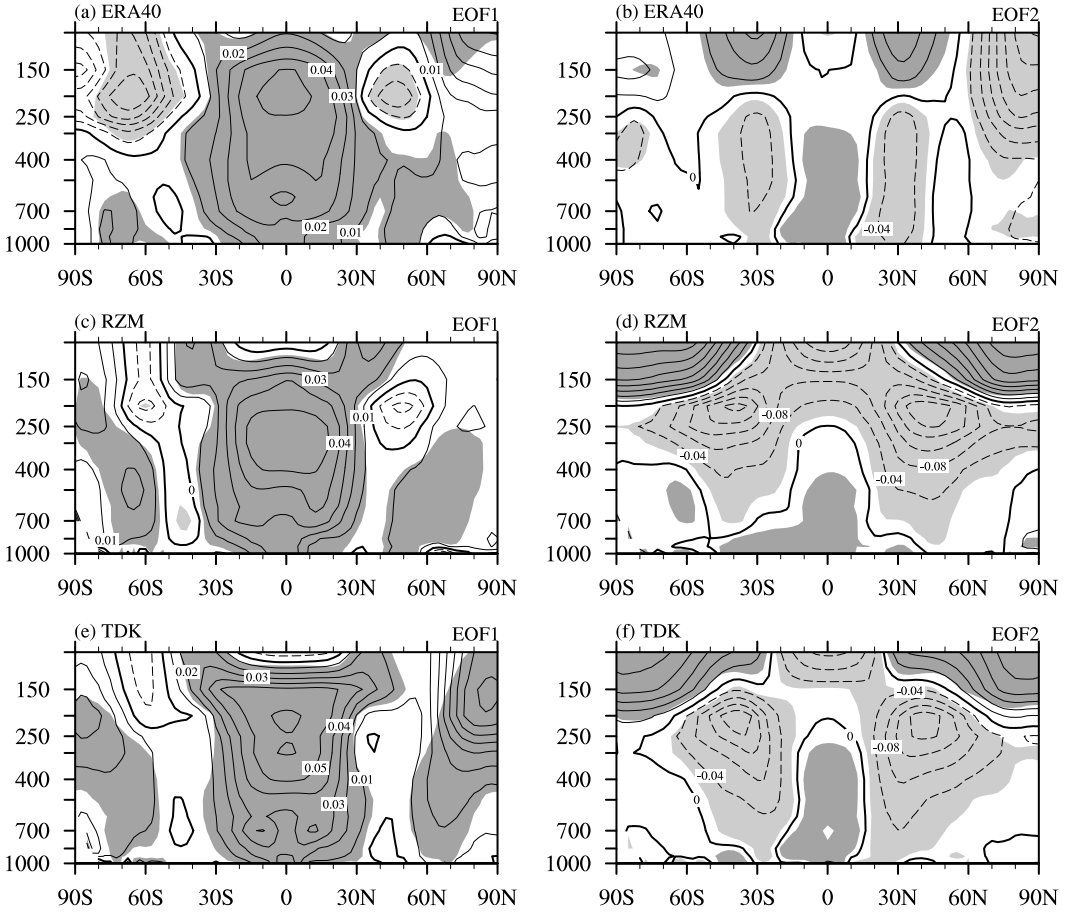

Fig. 3. The regression patterns for zonal mean temperature anomalies of EOF1 (left) and EOF2 (right), corresponding to the PCs shown in Fig. 4. The shading outlines the regions exceeding the 95% confidence limit by using Student's t-test. Units: K.

spheres.

The accompanying time series of the principal component (PC) of the first and second EOF modes derived from the ERA-40 reanalysis and the simulations are shown in Fig. 4. These two modes are orthogonal and represent different types of El Niño (Trenberth and Smith, 2006): the first mode represents the main ENSO events including the strong El Niño events in 1982/83, 1986/87, and 1997/98 in contrast to the La Niña in 1988/1989; the second mode captures the prolonged warm ENSO phase in the early 1990s, which is missing from the first mode. The 1997/98 El Niño signal is smaller in PC2 than in PC1. Both RZM and TDK can reasonably capture the canonical El Niño events presented by EOF-1. The temporal correlations with the reanalysis are 0.83 in RZM and 0.79 in TDK, both are statistically significant at the 1% level. For EOF-2, the temporal correlations with the reanalysis are 0.24 in RZM and 0.53 in TDK, indicating a substantially lower skill in the RZM run. The large spread of the PC2 time series results suggests the significant impact of the convection schemes. Previous studies have indicated the sensitivity of the tropical variability to the convective scheme (e.g., Slingo, 1987; Liu et al., 2005). Our results confirm this suggestion from the perspective of ENSO-related temperature changes.

The lead-lag correlation coefficient between the PCs and the Niño 3.4 SST index are calculated (Fig. 5). The first mode in ERA-40 shows the maximum positive correlation coefficient (exceeding 0.65) with the Niño SST leading by 3 to 4 months. This feature is well captured in both sets of SAMIL simulations. On the other hand, the second mode in the reanalysis shows the maximum positive correlation coefficient with the Niño 3.4 index at zero lag (about 0.58). The result of the TDK run is considerably better than that of the RZM run, with a correlation coefficient of 0.52 versus 0.28.

3.2 *The corresponding spatial temperature anomalies at four typical levels*

The geographic patterns of temperature at various

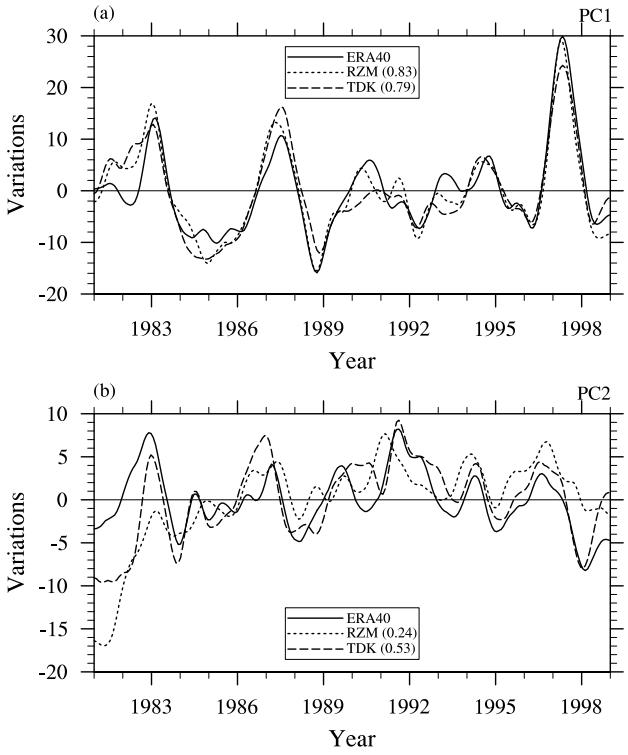

Fig. 4. Principal components (PC) time series for 1981–1999, obtained from the ERA40 reanalysis (solid lines), RZM (dot lines), and TDK (dashed lines): (a) PC1, (b) PC2. The third mode in the ERA-40 reanalysis is considered here as the second leading mode. The numbers in the parentheses following experiments' name show their correlation coefficients with the corresponding results in the reanalysis. All the curves are smoothed by the 11-point Trenberth filter (Trenberth, 1984) to highlight the fluctuations with periods for more than 8 months. The original PCs are used in all the regression and correlation analyses.

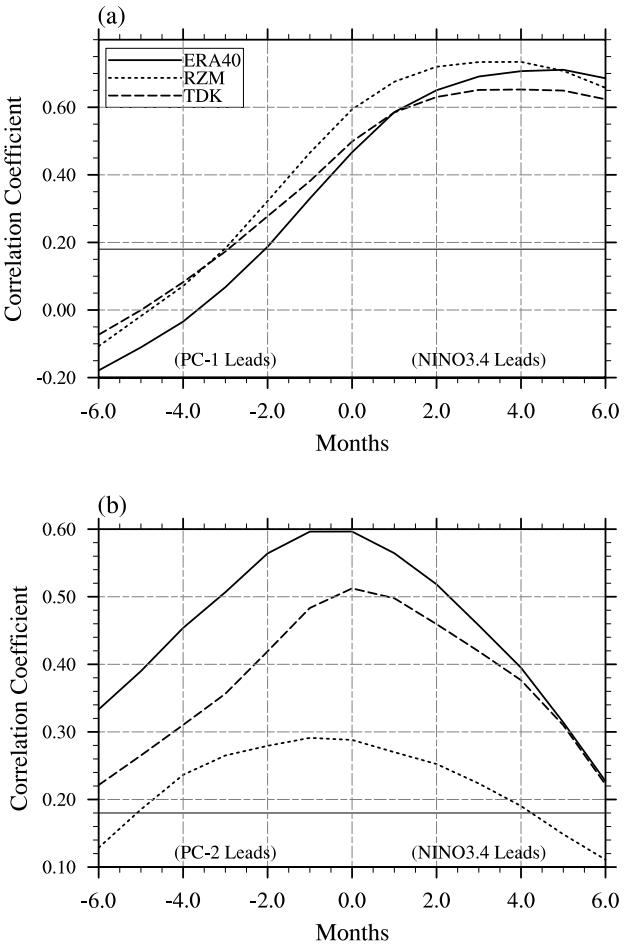

Fig. 5. Lag-correlation of NINO3.4 index with the (a) first principal components and (b) second principal components. The beeline indicates the 5% significance level using Student's t-test.

levels are revealed by regressing the temperature anomalies upon the corresponding PCs (Fig. 6). For EOF-1, the strongest warming anomalies at sea surface level are observed in the Indian Ocean, tropical eastern Pacific, and tropical Atlantic Ocean. The boomerang-shaped cooling anomalies, extending from the western Pacific into the central subtropical Pacific in both hemispheres are also evident. The warming is significant throughout the tropics, especially over the eastern Pacific. At 100 hPa, the anomalies over the tropical eastern Pacific are reversed, in opposition to the warming over the tropical western Pacific. The temperature anomalies at each level are reasonably reproduced in both the RZM and TDK runs, including the distinctive temperature structures at the sea surface level, the strong warming signals at 500 hPa and 300 hPa, as well as the cooling dipole at 100 hPa aloft the eastern Pacific straddling the equator.

For EOF-2, the tropical eastern Pacific warming is wider than for EOF-1 and extends poleward along the west coasts of the North and South American continents at the sea surface level (Fig. 7). The boomerang-shaped cooling in the western Pacific is also evident and stronger in this mode. Both the eastern Pacific warming and western Pacific cooling straddling the equator develop with height in the troposphere and turn to an opposite sign at 100 hPa. The spatial distributions associated with EOF-2 are more difficult to reproduce than EOF1. In RZM, the strengths of the temperature anomalies are underestimated at the sea surface level and 500 hPa, but overestimated in mid-high latitudes and more zonally distributed at 300 hPa and 100 hPa. The warming dipole above the eastern Pacific and the cooling dipole above the western Pacific in the mid-troposphere are also obscure in RZM. On the other hand, the TDK run is more skillful in capturing the spatial distributions of temperature anoma-

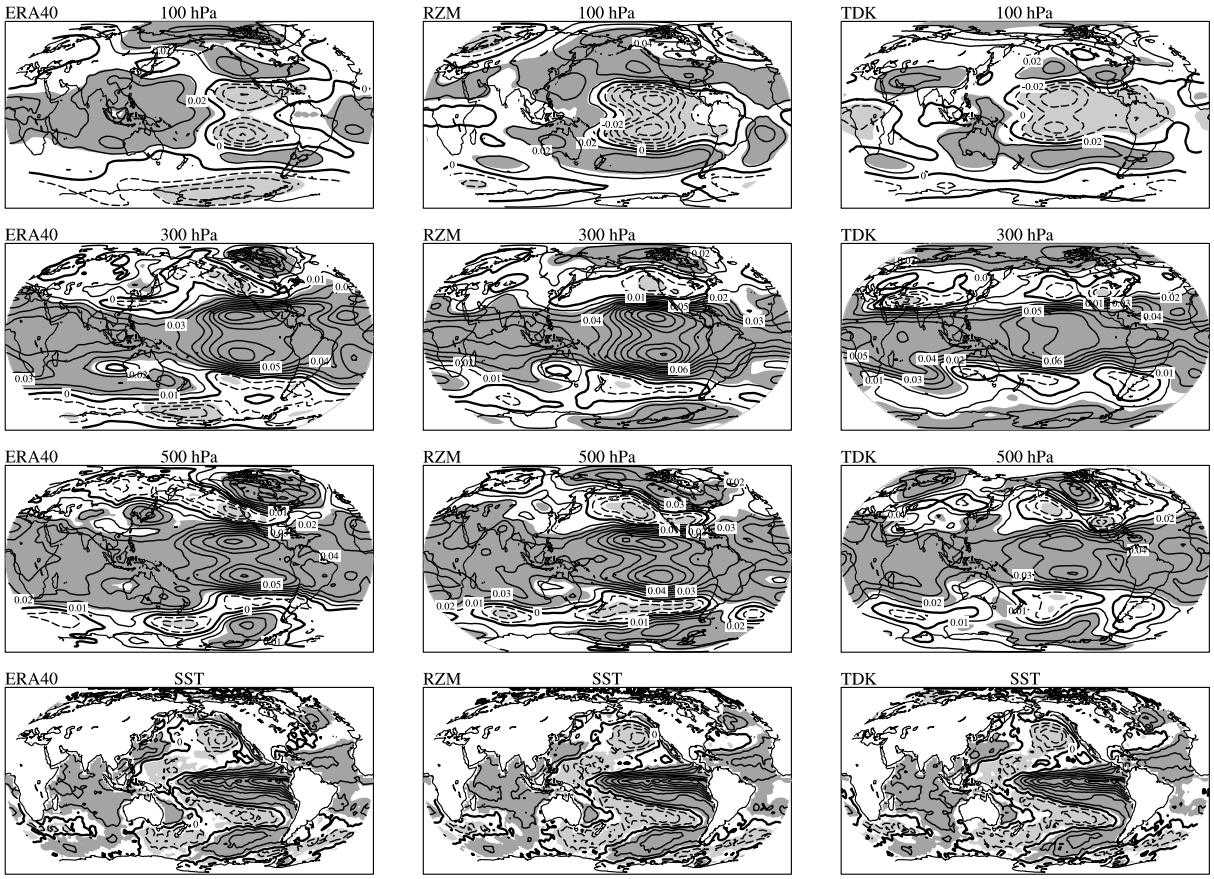

Fig. 6. For EOF-1, regression maps of temperature at sea surface level, 500 hPa, 300 hPa, and 100 hPa. The corresponding results for ERA40 reanalysis data, RZM, and TDK are, respectively, represented in the columns from left to right. Areas exceeding a significance limit of 5% using Student's t-test are shaded.

lies, including the warming in the central-eastern tropical Pacific, the strong negative sign in the western tropical Pacific at the sea surface level, as well as the quadrupole temperature anomalies at 500 hPa and 300 hPa.

Overall, both RZM and TDK reasonably capture spatial temperature features at the four core levels associated the first mode. However, the second mode is more difficult to reproduce in the model and is more sensitive to the choice of convection schemes.

4. Discussion

The large-scale circulation and precipitation changes are closely relevant to the reproduction of temperature variability and are discussed in this section.

4.1 *The associated sea level pressure changes*

For EOF-1, the pressure gradients between the eastern and western tropical Pacific are evident (Fig. 8a). This Southern Oscillation (SO) like pressure structure in tropics can be reasonably reproduced, especially for the characteristic high pressure anomalies in the western tropical Pacific, extending into the subtropical Pacific in both hemispheres. For EOF-2, the see-saw pattern of sea level pressure (SLP) between the eastern and western tropical Pacific with maxima off the equator is closer to the classical SO pattern (Fig. 8b). The anomalies are underestimated in RZM, especially in the western and northeastern Pacific. The poor SLP reproduction in RZM is associated with the unrealistic temperature anomalies in the lower troposphere (Fig. 7) and the precipitation anomalies (Fig. 9). The mid-latitudinal negative pressure anomalies straddling the equator in the eastern Pacific associated with EOF-2 are well represented in TDK and are in good agreement with the reanalysis.

4.2 *The associated precipitation and Walker circulation changes*

For EOF-1, the associated precipitation anomalies are strongest in the equatorial region, as shown by the anomalous precipitation in the central-eastern tropical Pacific and negative precipitation anomalies in the

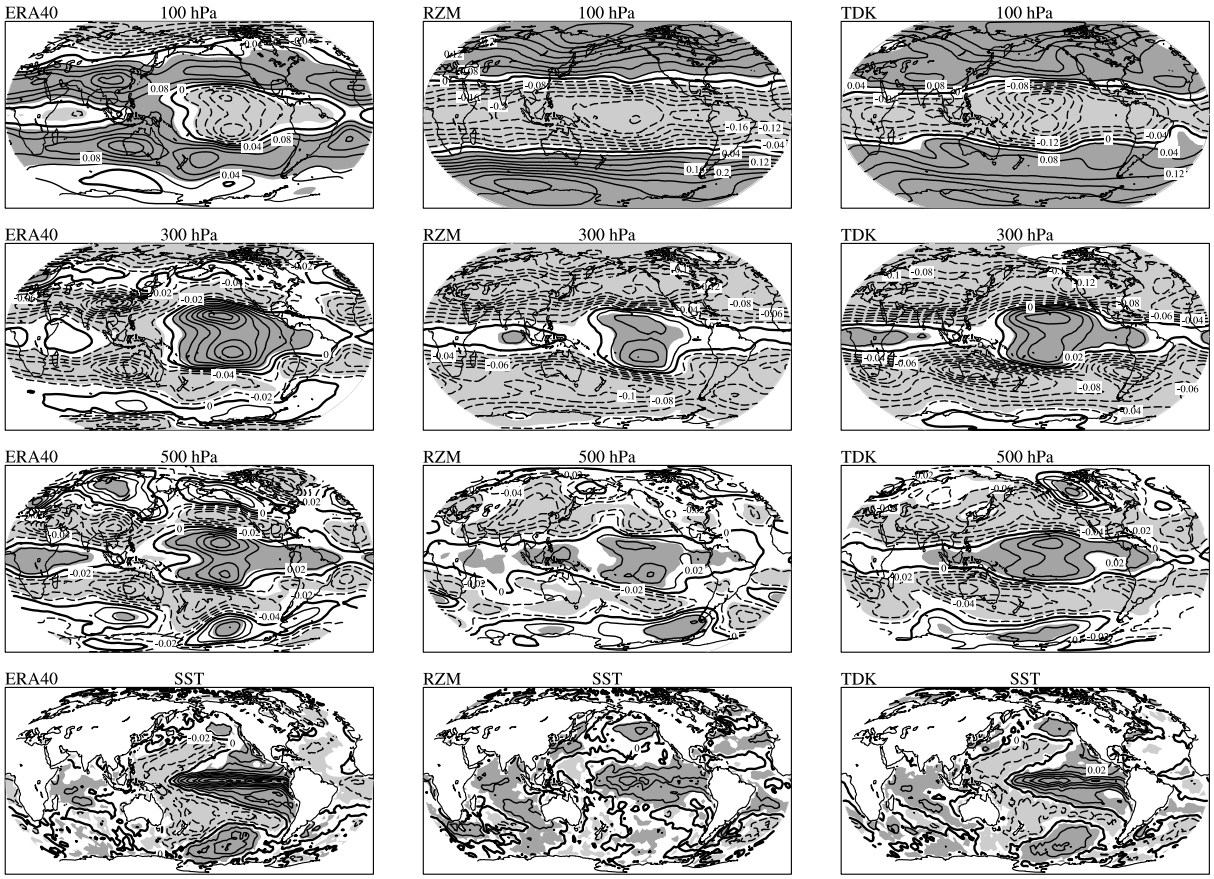

Fig. 7. Same as in Fig. 6, but for EOF-2.

western Pacific extending to the subtropics in both hemispheres (Fig. 9a). Both simulations are able to capture these features (Fig. 9c, Fig. 9e), despite stronger precipitation in the central-eastern Pacific in RZM and a westward extension of the rain belt in TDK. For EOF-2, the anomalous precipitation center moves to the central tropical Pacific and the western Pacific is dominated by lower than climatological rainfall levels (Fig. 9b). The characteristic precipitation anomalies are distorted in RZM, wherein the anomalous precipitation center is located near the date line. Despite the westward extension of a positive precipitation anomaly center, the TDK run can reasonably reproduce the precipitation anomalies in the tropics.

The vertical cross sections of the zonal wind and vertical pressure velocity (ω) anomalies averaged along the equator from 10°S to 10°N are shown in Fig. 10. The ascent and decent anomalies occur over regions with excessive/deficient precipitation compared to climatology. Coherent changes are seen between the Walker circulation and precipitation. For EOF-1, the ascent anomalies extend from the eastern Pacific to the date line where there is exaggerated equatorial precipitation (Fig. 10a). The easterlies in the upper troposphere are favorable to the stronger convection and contribute to the abundant precipitation. Compared with the reanalysis, vertical motions and easterly anomalies in the upper troposphere are stronger in RZM (Fig. 10b), leading to exaggerated precipitation along the central eastern tropical Pacific. The TDK run is able to capture the main features of the convective anomalies (Fig. 10c), although the convection center extends westward in accordance with the precipitation bias (Fig. 9e). The easterly anomalies in upper troposphere are underestimated in TDK.

The subtropical precipitation anomalies in EOF-2 are also significant, corresponding to the classical SO shown in Fig 8b, as well as the poleward extension of the warming along the western coasts of the North and South American continents (Fig. 7). The expanded precipitation anomalies are more reasonably reproduced in TDK, indicating the advantage of the Tiedtke scheme in simulating the atmospheric variability in the off-equatorial region. By examining the performances of different convection schemes in the tropical atmosphere, Liu et al. (2009) found that the precipitation is confined to the equator when using the Zhang and McFarlane convective scheme but extended

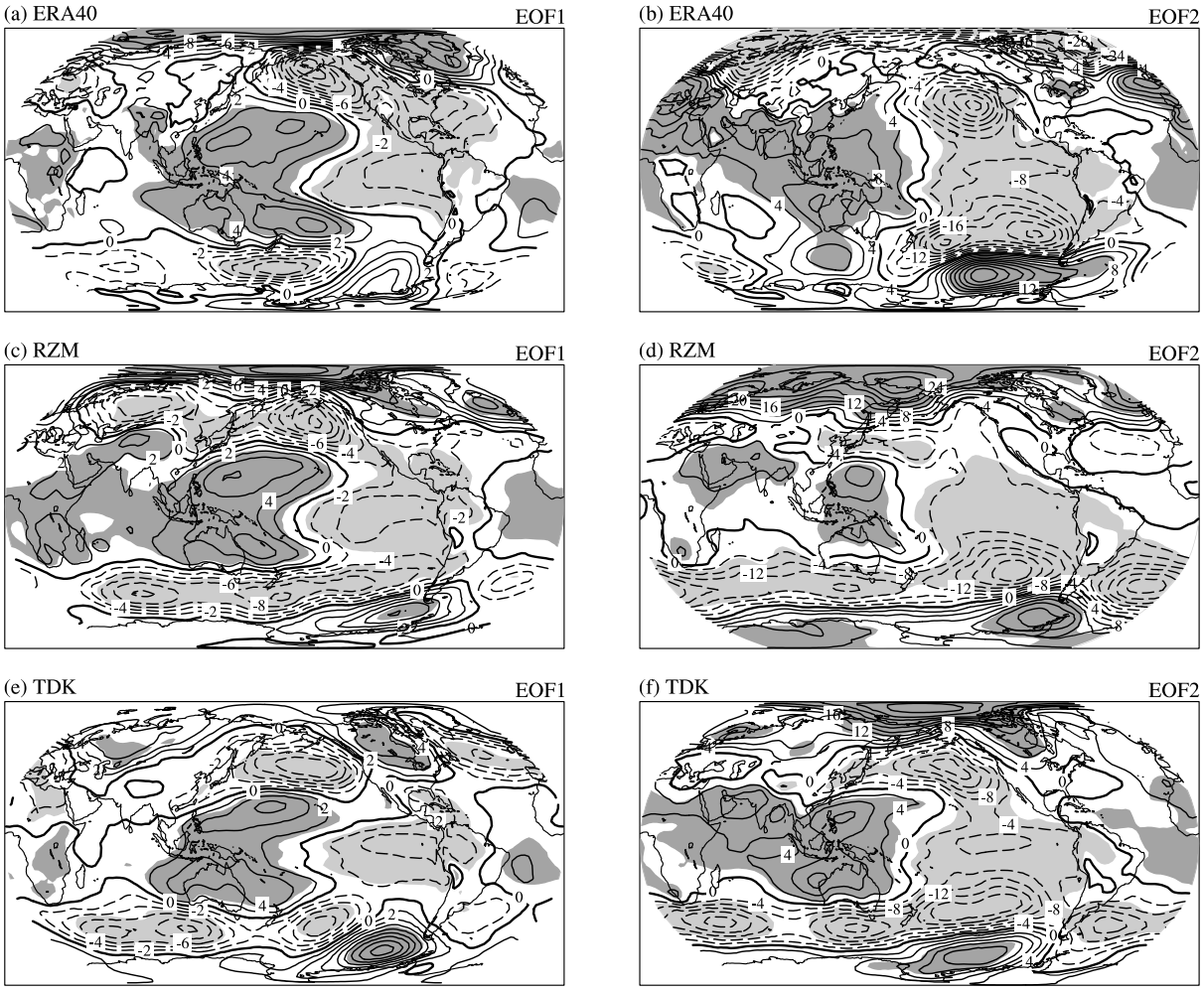

Fig. 8. Regression maps of the first (left) and second (right) EOF principal components with sea level pressure anomalies. (a) and (b) ERA40, (c) and (d) RZM, (e) and (f) TDK. Units: Pa. Shaded regions are statistically significant at the 5% level according to Student's t-test.

poleward when using the Tiedtke scheme. They argue that the different precipitation patterns may be caused by the different triggering conditions for deep convection in the two schemes. In Tiedtke, the evaporation-wind positive feedback off the equator favors the development of convective precipitation on either side of the equator (Liu et al., 2010).

Corresponding to the "dry-wet-dry" tripole anomalous rainfall centers in the western Pacific, central Pacific, and tropical Atlantic Ocean, respectively, strong areas of descent and ascent are evident along the equator in EOF-2 (Fig. 10d). Strong anomalous vertical motions are evident over the tropical central and western Pacific in accordance with the divergent wind anomalies in the upper troposphere. The anomalous vertical motions and the associated upper tropospheric zonal winds are underestimated and constrained in the central Pacific in RZM (Fig. 10e) associated with the unrealistic precipitation anomalies (Fig. 9d). On the other hand, the TDK run shows reasonable simulations of precipitation anomalies (Fig. 9f), three vertical motion centers, as well as the anomalous zonal winds in the upper troposphere (Fig. 10f).

The positive/negative precipitation anomalies directly contribute to latent heat release and the spatial temperature distributions. The geographical and temporal variability in stratiform rain play an important role in shaping the structure of the large-scale tropical circulation (Schumacher et al., 2004). Higher fractions of stratiform rain are associated with an elevated level of maximum heating and a stronger upper-level response (Houze, 1982, 1989; Hartmann et al., 1984; Schumacher et al., 2004). The partition between the convective and stratiform rain is very sensitive to the cumulus schemes (Liang et al., 2004b). As shown in Figs. 3, 6, and 7, the temperature biases are more significant in the upper troposphere, especially for RZM.

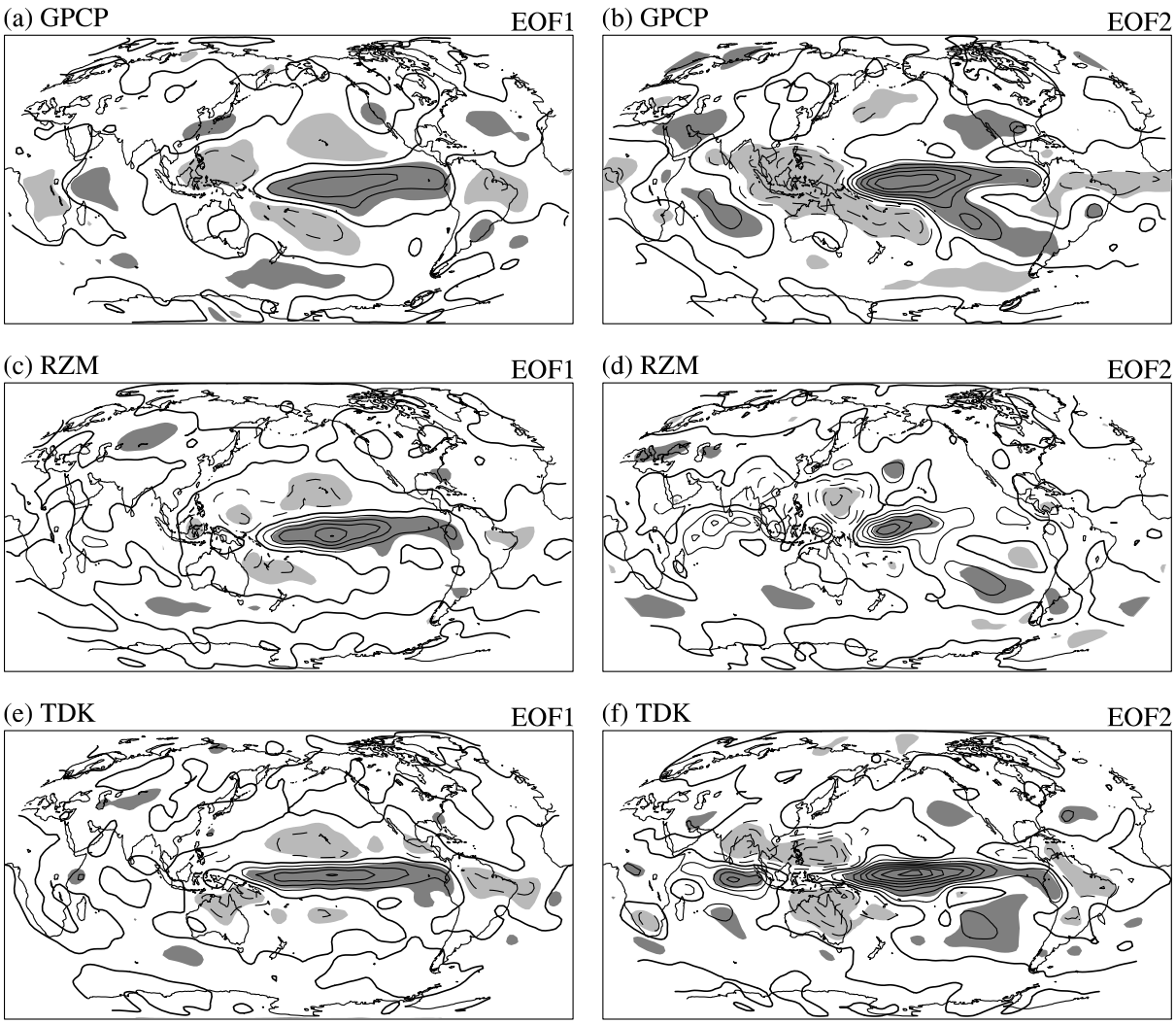

Fig. 9. Regression maps of precipitation anomalies against the first (left) and second (right) EOF principal component. (a) and (b) ERA40, (c) and (d) RZM, (e) and (f) TDK. Shaded regions are statistically significant at the 5% level according to Student's t-test. Contour interval is 0.05 mm d^{-1}.

Based on the temperature bias result, the ability of SAMIL to reproduce the stratiform rain fraction deserves further investigation.

5. Conclusion

Two different convection schemes are employed in a spectral AGCM (SAMIL) to test the impacts of convection schemes on capturing the vertical atmospheric temperature anomalies associated with two types of El Niño. The El Niño signals are derived from the tropical vertical temperature anomalies using EOF analysis. The EOF-1 pattern represents the canonical El Niño and the EOF-2 pattern represents the atypical El Niño characterized by the prolonged El Niño events during the early 1990s.

Two sets of AMIP-type simulations covering the period from January 1976 to December 1999 are carried out. The two SAMIL simulations were driven by identical SST but employed two different convection schemes, namely the revised Zhang and Macfarlane (RZM) and the Tiedtke (TDK) convection schemes.

The dominant EOF mode highlighting the canonical El Niño is reasonably simulated by SAMIL, although the observed mid-latitude cooling centers in the upper troposphere in both hemispheres are insignificant in both the RZM and TDK runs. The performance of the model in simulating the EOF-2 mode is sensitive to the convection scheme. In the RZM run, neither the strength nor the pattern of temperature anomalies are realistic, including the existence of SST anomalies that are too weak in the eastern and western Pacific and the obscured off-equator quadrupole temperature anomalies at 500 hPa and 300 hPa.

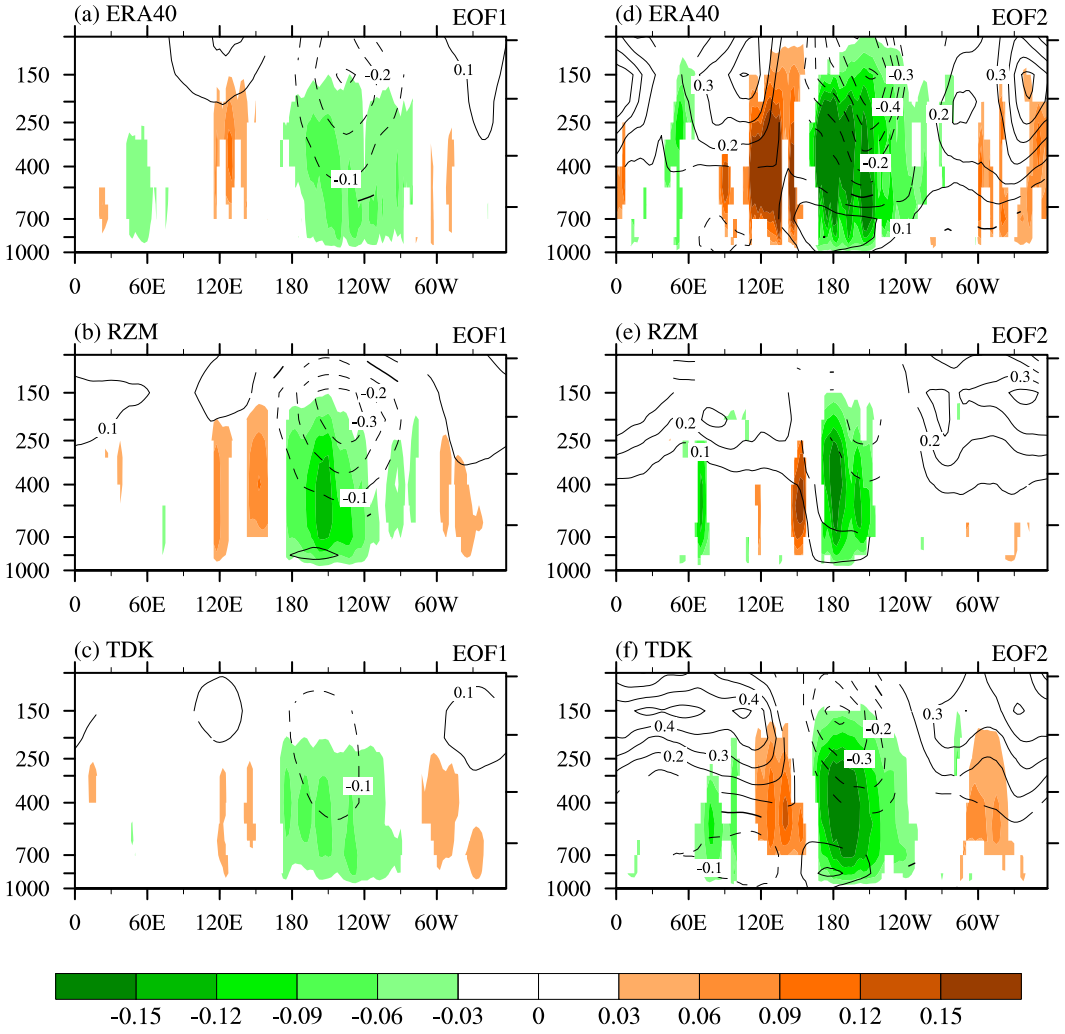

Fig. 10. Regression patterns of the anomalous zonal-pressure circulation averaged from 10°S to 10°N associated with the first (left) and second (right) EOF principal component. The vertical motion is shaded (units: 10^{-2} Pa s^{-1}) and the contours represent the zonal wind (units: m s^{-1}). Only the values statistically significant at the 5% level according to Student's t-test are shown.

The TDK run exhibits a better performance in these regards.

The large-scale anomalous circulation fields also show similar strengths and weaknesses. The SLP gradients between the eastern and western tropical Pacific associated with EOF-1 are reasonably captured. The classical SO pattern in EOF-2 is well presented in the TDK run. When employing the RZM scheme, the positive/negative pressure anomalies over the western/northeastern Pacific are underestimated in accordance with the unrealistic anomalous precipitation. The deficiency of RZM in reproducing the strong descents and ascents over the tropical Pacific is consistent with the overly weak zonal wind anomalies in the upper troposphere.

Acknowledgements. This work was jointly supported by the National Natural Science Foundation of China (40890054, 40821092, 90711004), R&D Special Fund for Public Welfare Industry (meteorology)(GYHY200706010), and National Key Technologies R&D Program (2007BAC29B03).

REFERENCES

Adler, R. F., and Coauthors, 2003: The version-2 global precipitation climatology project (GPCP) monthly precipitation analysis (1979–present). *J. Hydrometeor.*, **4**, 1147–1167.

Arakawa, A., 2004: The cumulus parameterization problem: Past, present, and future. *J. Climate*, **17**, 2493–2525.

Arakawa, A., and W. H. Schubert, 1974: Interaction of a cumulus cloud ensemble with the large-scale environment, Part I. *J. Atmos. Sci.*, **31**, 674–701.

Bao, Q., Y. M. Liu, T. J. Zhou, Z. Z. Wang, G. X. Wu and P. F. Wang, 2006: The sensitivity of the spectral atmospheric general circulation model of LASG/IAP to the land process. *Chinese J. Atmos. Sci.*, **30**(6), 1077–1090. (in Chinese)

Bonan, G. B., 1998: The land surface climatology of the NCAR Land Surface Model coupled to the NCAR Community Climate Model. *J. Climate*, **11**, 1307–1326.

Chen, H., T. Zhou, and R. Yu, 2009: The East Asian summer monsoon simulated by.coupled model FGOALS_s. *Chinese J. Atmos. Sci.*, **33**(1), 155–167. (in Chinese)

Chen, H., T. Zhou, R. B. Neale, X. Wu, and G. J. Zhang, 2010: Performance of the New NCAR CAM3.5 in East Asian Summer Monsoon Simulations: Sensitivity to Modifications of the Convection Scheme. *Journal of Climate*, **23**, 3657–3675.

Dai, F. S., R. C. Yu, X. H. Zhang, and Y. Q. Yu, 2005: A statistically-based low-level cloud scheme and its tentative application in a general circulation model. *Acta Meteorologica Sinica*, **19**, 263–274.

Edwards, J. M., and A. Slingo, 1996: Studies with a flexible new radiation code. 1. Choosing a configuration for a large-scale model. *Quart. J. Roy. Meteor. Soc.*, **122**, 689–719.

Fernández, J., J. P. Montávez, J. Sáenz, J. F. González-Rouco, and E. Zorita, 2007: Sensitivity of the MM5 mesoscale model to physical parameterizations for regional climate studies: Annual cycle. *J. Geophys. Res.*, **112,** D04101, doi: 10.1029/2005JD006649.

Giorgi, F., and C. Shields, 1999: Tests of precipitation parameterizations available in latest version of NCAR regional climate model (RegCM) over continental United States. *J. Geophys. Res.*, **104**(D6), 6353–6375.

Hack, J. J., 1994: Parameterization of moist convection in the National Center for Atmospheric Research community climate model (CCM2). *J. Geophys. Res.*, **99** (D3), 5551–5568.

Hartmann, D. L., H. H. Hendon, and R. A. Houze Jr., 1984: Some implications of the mesoscale circulations in tropical cloud clusters for large-scale dynamics and climate. *J. Atmos. Sci.,* **41,** 113–121.

Houze, R. A. Jr., 1982: Cloud clusters and large-scale vertical motions in the tropics. *J. Meteor. Soc. Japan,* **60**, 396–410.

Houze, R. A. Jr., 1989: Observed structure of mesoscale convective systems and implications for large-scale heating. *Quart. J. Roy. Meteor. Soc.*, **115**, 425–461.

Johns, T., and Coauthors, 2004: HadGEM1—Model description and analysis of preliminary experiments for the IPCC Fourth Assessment Report, Hadley Centre Technical Note 55, Met office, Exeter, U. K, 75pp.

Li, B., T. Zhou,C. Wu, and Q. Bao, 2009: Relationship between rainfall and sea surface temperature simulated by LASG/ IAP AGCM and CGCM. *Chinese J. Atmos. Sci.*, **33**(5), 1071–1086. (in Chinese)

Li, H., T. Zhou, and C. Li, 2010: Decreasing trend in global land monsoon precipitation over the past 50 years simulated by a coupled climate model. *Adv. Atmos. Sci.*, **27**(2), 285–292.

Liang, X. Z., L. Li, A. Dai, and K. E. Kunkel, 2004a: Regional climate model simulation of summer precipitation diurnal cycle over the United States. *Geophys. Res. Lett.*, **31**, L24208, doi: 10.1029/2004GL021054.

Liang, X. Z., L. Li, K. E. Kunkel, M. Ting, and J. X. L. Wang, 2004b: Regional Climate Model Simulation of U.S. Precipitation during 1982–2002. Part I: Annual Cycle. *J. Climate*, **17**, 3510–3529.

Liu, K., 2008: Bias analyses of the modeled tropical precipitation and its improvement. Ph. D. dissertation, Institute of Atmospheric Physics, Chinese Academy of Sciences, 162pp. (in Chinese)

Liu, P., B. Wang, K. R. Sperber, T. Li, and G. A. Meehl, 2005: MJO in the NCAR CAM2 with the Tiedtke Convective Scheme. *J. Climate*, **18**, 3007–3020.

Liu, Y. M., L. Guo, G. X. Wu, and Z. Z. Wang, 2010: Sensitivity of ITCZ configuration to cumulus convective parameterizations on an aqua planet. *Climate Dyn.*, **34**, 223–240.

North, G. R., T. L. Bell, R. F. Cahalan, and F. J. Moeng, 1982: Sampling Errors in the Estimation of Empirical Orthogonal Functions. *Mon. Wea. Rev.*, **110**, 699–706.

Onogi, K., and Coauthors, 2007: The JRA-25 Reanalysis. *J. Meteor. Soc. Japan*, **85**, 369–432.

Rayner, N. A., D. E. Parker, E. B. Horton, C. K. Folland, L. V. Alexander, D. P. Rowell, E. C. Kent, and A. Kaplan, 2003: Global analyses of sea surface temperature, sea ice, and night marine air temperature since the late nineteenth century. *J. Geophys. Res.*, **108**(D14), 4407, doi: 10.1029/2002JD002670.

Schumacher, C., R. A. Houze, and I. Kraucunas, 2004: The tropical dynamical response to latent heating estimates derived from the TRMM precipitation radar. *J. Atmos. Sci.*, **61**, 1341–1358.

Slingo, J. J., 1987: The development and verification of a cloud prediction scheme for the ECMWF model. *Quart. J. Roy. Meteor. Soc.*, **213**, 899–927.

Song, X. L., 2005: The evaluation analysis of two kinds of mass-flux cumulus parameterization in climate simulation. Ph. D. dissertation, Institute of Atmospheric Physics, Chinese Academy of Sciences, 158pp. (in Chinese)

Takemura, T., H. Okamoto, Y. Maruyama, A. Numaguti, A. Higurashi, and T. Nakajima, 2000: Global three-dimensional simulation of aerosol optical thickness distribution of various origins. *J. Geophys. Res.*, **105**(D14), 17853–17873.

Tiedtke, M., 1989: A comprehensive mass flux scheme for cumulus parameterization in large-scale models. *Mon. Wea. Rev.*, **117**, 1779–1800.

Trenberth, K. E., 1984: Signal versus noise in the southern oscillation. *Mon. Wea. Rev.*, **112**, 326–332.

Trenberth, K. E., and L. Smith, 2006: The vertical structure of temperature in the tropics: Different flavors of El Nino. *J. Climate*, **19**, 4956–4970.

Trenberth, K. E., and L. Smith, 2009: Variations in the three-dimensional structure of the atmospheric circulation with different flavors of El Niño. *J. Climate*, **22**, 2978–2991.

Uppala, S. M., and Coauthors, 2005: The ERA-40 reanalysis. *Quart. J. Roy. Meteor. Soc.*, **131**, 2961–3012.

Wang, B., X. Xie, and L. Li, 2009: A review on aspects of climate simulation assessment. *Adv. Atmos. Sci.*, **26**, 736–747.

Wu, B., T. Zhou, T. Li, and Q. Bao, 2009: Interannual variability of the Asian-Australian monsoon and ENSO simulated by an ocean-atmosphere coupled model. *Chinese J. Atmos. Sci.*, **32**(2), 285–299. (in Chinese)

Xu, Y., X. Gao, and F. Giorgi, 2009: Regional variability of climate change hot-spots in East Asia. *Adv. Atmos. Sci.*, **26**, 783–792.

Yhang, Y. B., and S. Y. Hong, 2008: Improved physical processes in a regional climate model and their impact on the simulated summer monsoon circulations over East Asia. *J. Climate*, **21**, 963–979.

Zhang, G. J., 1994: Effects of cumulus convection on the simulated monsoon circulation in a aeneral-circulation model. *Mon. Wea. Rev.*, **122**, 2022–2038.

Zhang, G. J., 2002: Convective quasi-equilibrium in midlatitude continental environment and its effect on convective parameterization. *J. Geophys. Res.*, **107**(D14), 4220, doi: 10.1029/2001JD001005.

Zhang, G. J., and N. A. McFarlane, 1995: Sensitivity of climate simulations to the parameterization of cumulus convection in the CCC-GCM. *Atmos.-Ocean*, **3**, 407–446.

Zhang, L., T. Zhou, B. Wu, and Q. Bao, 2008: The annual modes of tropical precipitation simulated by LASG/IAP ocean atmosphere coupled model Fgoals_s1.1 *Acta Meteorologica Sinica*, **66**, 968–981. (in Chinese)

Zhou, T. J., R. C. Yu, Z. Z. Wang, and T. W. Wu, 2005a: *The Atmospheric General Circulation Model SAMIL and Its Associated Coupled Climate System Model FGOALS-s*. China Meteorological Press, 288pp. (in Chinese)

Zhou, T., and Coauthors, 2005b: The climate system model FGOALS-S using LASG/IAP spectral AGCM SAMIL as its atmospheric component. *Acta Meteorologica Sinica*, **63**(5), 702–715. (in Chinese)

Zhou, T. J., Y. Yu, H. L. Liu, W. Li, X. B. You, and G. Q. Zhou, 2007: Progress in the development and application of climate ocean models and ocean-atmosphere coupled models in China. *Adv. Atmos. Sci.*, **24**, 1109–1120, doi: 10.1007/s00376-007-1109-3.

Zhu, J. H., and X. Z. Liang, 2007: Regional climate model simulations of US precipitation and surface air temperature during 1982–2002: Interannual variation. *J. Climate*, **20**, 218–232.